Manthey, J., & Hagar, L. P. (1985) *J. Biol. Chem. 260*, 9654-9659.
Manthey, J., Boldt, N. J., Bocian, D. F., & Chan, S. I. (1986) *J. Biol. Chem. 261*, 6734-6741.
Newton, N., Morell, D. B., Clarke, L., & Clezy, P. S. (1965) *Biochim. Biophys. Acta 96*, 476-486.
Odajima, T., & Yamazaki, I. (1970) *Biochim. Biophys. Acta 206*, 71-77.
Oertling, W. A., & Babcock, G. T. (1988) *Biochemistry 27*, 3331-3338.
Ozaki, Y., Iriyama, K., Ogoshi, H., Ochiai, T., & Kitagawa, T. (1986a) *J. Phys. Chem. 90*, 6105-6112.
Ozaki, Y., Iriyama, K., Ogoshi, H., Ochiai, T., & Kitawaga, T. (1986b) *J. Phys. Chem. 90*, 6113-6118.
Proniewicz, L. M., Bajdor, K., & Nakamoto, K. (1986) *J. Phys. Chem. 90*, 1760-1766.
Rakhit, G., & Spiro, T. G. (1976) *Biochem. Biophys. Res. Commun. 71*, 803-808.
Renganathan, V., & Gold, M. H. (1986) *Biochemistry 25*, 1626-1631.
Schultz, J., & Schmukler, H. W. (1964) *Biochemistry 3*, 1234-1238.
Sibbett, S. S., & Hurst, J. D. (1984) *Biochemistry 23*, 3007-3013.
Sitter, A. J., Reczek, C. M., & Terner, J. M. (1985) *J. Biol. Chem. 260*, 7515-7522.
Spiro, T. G., Stong, J. D., & Stein, P. (1979) *J. Am. Chem. Soc. 101*, 2648-2655.
Stelmaszyńska, T., & Zgliczyński, J. M. (1974) *Eur. J. Biochem. 45*, 305-312.
Stump, R. F., Deanin, G. G., Oliver, J. M., & Shelnutt, J. A. (1987) *Biophys. J. 51*, 605-610.
Terner, J., Sitter, A. J., & Reczek, C. M. (1985) *Biochim. Biophys. Acta 828*, 73-80.
Wever, R., & Plat, H. (1981) *Biochim. Biophys. Acta 661*, 235-239.

A Nuclear Overhauser Effect Study of the Heme Crevice in the Resting State and Compound I of Horseradish Peroxidase: Evidence for Cation Radical Delocalization to the Proximal Histidine†

V. Thanabal,‡ Gerd N. La Mar,*,‡ and Jeffrey S. de Ropp§
Department of Chemistry and UCD NMR Facility, University of California, Davis, California 95616
Received January 27, 1988; Revised Manuscript Received March 24, 1988

ABSTRACT: The assignment of resolved hyperfine-shifted resonances in high-spin resting state horseradish peroxidase (HRP) and its double-oxidized reactive form, compound I (HRP-I), has been carried out by using the nuclear Overhauser effect (NOE) starting with the known heme methyl assignments in each species. In spite of the efficient spin–lattice relaxation and very broad resonances, significant NOEs were observed for all neighboring pyrrole substituents, which allowed the assignment of the elusive propionate α-methylene protons. In the resting state HRP, this leads directly to the identity of the proximal His-170 H_β peaks. The determination that one of the most strongly contact-shifted single proton resonances in HRP-I *does not* arise from the porphyrin dictates that the cation radical must be delocalized to some amino acid residue. The relaxation properties of the non-heme contact-shifted signal in HRP-I support the identity of this contributing residue as the proximal His-170. Detailed analysis of changes in both contact shift pattern and NOEs indicates that compound I formation is accompanied by a $\sim 5°$ rotation of the 6-propionate group. The implication of a porphyrin cation radical delocalized over the proximal histidine for the proposed location of the solely amino acid centered radical in compound I of related cytochrome *c* peroxidase is discussed.

Horseradish peroxidase, HRP,[1] is one of a number of functionally related heme enzymes for which the high-spin ferric resting state reacts with hydrogen peroxide to yield an initially reactive species two oxidizing equivalents above the resting state (Dunford, 1982; Dunford & Stillman, 1976; Morrison & Schonbaum, 1976). One of these oxidizing equivalents is invariably associated with oxidation of the iron center to Fe^{IV} (usually as the ferryl ion, Fe^{IV}=O) that is retained in compound II, with the second one residing on an organic moiety. For HRP compound I, HRP-I, optical spectra have been found characteristic for a porphyrin cation radical (Dolphin et al., 1971), while yeast cytochrome *c* peroxidase compound I, C*c*P-I, has been shown to possess a free radical on an amino acid side chain removed from the iron (Yonetani & Ray, 1965). While there is a paucity of hard structural information on HRP, the yeast cytochrome *c* peroxidase, C*c*P, has yielded to successful X-ray crystallographic structural analysis for both its resting-state C*c*P and compound I, C*c*P-I (Poulos & Kraut, 1980; Finzel et al., 1984; Edwards et al., 1987).

Solution NMR studies have been found particularly useful for delineating a number of structural features of the heme cavity of HRPCN, the cyanide complex of the resting state (Thanabal et al., 1987a,b, 1988), which could be interpreted

† This work was supported by a grant from the National Institutes of Health, GM 26226.
* Address correspondence to this author.
‡ Department of Chemistry.
§ UCD NMR Facility.

[1] Abbreviations: HRP, horseradish peroxidase; HRP-I, compound I of horseradish peroxidase; C*c*P, cytochrome *c* peroxidase; C*c*P-I, compound I of cytochrome *c* peroxidase; NMR, nuclear magnetic resonance; NOE, nuclear Overhauser effect; DSS, 2,2-dimethyl-2-silapentane-5-sulfonate.

0006-2960/88/0427-5400$01.50/0

on the basis of sequencing homology to CcP (Welinder, 1985; Sakurada et al., 1986). These studies were based on successful extensions to paramagnetic systems of the nuclear Overhauser effect, NOE (Noggle & Schirmer, 1971), for both resonance assignment and structural determination, relying on previously reported assignments of heme methyl peaks on the basis of isotope labels (La Mar et al., 1980a; de Ropp et al., 1984). More recently, we have shown that such NOE techniques can be extended even further to resting-state HRP and HRP-I, allowing the determination of the orientation of vinyl side chains (Thanabal et al., 1986).

In this paper, we explore further the utility of NOEs for structural determination in strongly paramagnetic derivatives, HRP ($S = {}^5/_2$) and HRP-I (Fe^{IV}, $S = 1$, weakly coupled to $S = {}^1/_2$ radical) (Dunford & Stillman, 1976). For the resting state HRP, we focus on the location and assignment of the α-methylene protons of hemin (I). Isotope labeling has revealed (La Mar et al., 1980b) the identity of all but six of the low-field single proton resonances, with only the four propionate H_α peaks of the heme unassigned. Since only the heme and the axial histidine (La Mar, 1979; Satterlee, 1986) can give rise to large contact shifts from the magnetically isotropic high-spin iron(III) center (La Mar & Walker-Jensen, 1978), assignment of the propionate H_αs will yield the elusive axial His-170 H_β signals expected to resonate in this window (Lauffer et al., 1983). The state of protonation of the axial histidyl imidazole (Morrison & Schonbaum, 1976; Nicholls, 1962) has been implicated in the mechanism of peroxidase activity.

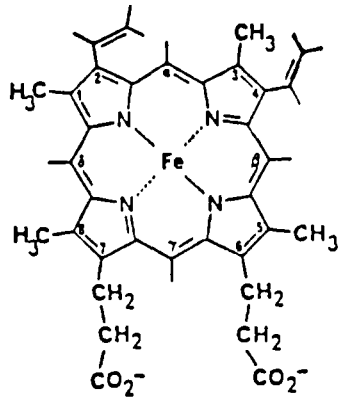

I

For HRP-I, isotope labeling has similarly identified (La Mar et al., 1981) all but the four heme propionate α-methylene signals. In this case, since only four strongly contact-shifted resonances remained unassigned, it was tacitly assumed (La Mar et al., 1981) that these four peaks must originate from the propionate H_αs. Conversely, if it can be established that the strongly shifted peaks do not all arise from the heme, then the view that the second oxidizing equivalent is localized completely on the porphyrin must be reassessed. Lastly, since hyperfine shifts in both resting state HRP and HRP-I are largely scalar or contact in origin (La Mar, 1979; Satterlee, 1986), the pattern of the methylene proton shifts for individual propionate groups can be interpreted in terms of their orientation relative to the heme plane (La Mar, 1973), and their orientation can be compared in HRP and HRP-I to assess structural changes that accompany compound I formation.

Experimental Procedures

Sample Preparation. HRP, type VI, was purchased from Sigma as a lyophilized salt-free powder; the protein is predominantly isozyme C. The detailed purification, activity assay, and electrophoretic characterization of the protein type used in this study have been published (La Mar et al., 1980b). Solutions for proton NMR studies were 3 mM in protein in 99.9% ^2H_2O. The solution pH was adjusted with 0.2 M ^2HCl or 0.2 M NaO^2H and was measured with a Beckman Model 3550 pH meter equipped with an Ingold microcombination electrode; pH values are not corrected for the isotope effect. Compound I was generated by the addition of 2 equiv of H_2O_2 to the resting-state HRP. The green species is stable for ~30 min at 15 °C. The optical spectrum of HRP-I is identical with that reported earlier (Dolphin et al., 1971).

Spin–Lattice Relaxation Time. Nonselective T_1s were determined by a variation of the standard inversion–recovery sequence to include a composite 180° pulse (Freeman et al., 1976). The transmitter carrier frequency was set at the middle of the downfield peaks to effect an efficient inversion of all the peaks. The T_1 values were computed by a nonlinear least-squares fit to

$$(I_\infty - I_t)/2I_\infty = A \exp(-t/T_1) \quad (1)$$

where I_t and I_∞ are the intensities of the resonances at t and $>5T_1$ after the 180° pulse and t is the delay, in milliseconds, between the 180° and 90° pulses.

Nuclear Overhauser Effect. The NOE, $\eta_{i\to j}$, is defined as (Noggle & Shirmer, 1971)

$$\eta_{i\to j} = (I_j - I_j^0)/I_i^0 \quad (2)$$

where I_j and I_j^0 are intensities of the signal from the detected proton H_j with and without saturating the resonance of the spin H_i. It is found that an irradiation time of 30 ms is close to the steady-state condition (eq 3) without significant spin diffusion (Thanabal et al., 1987a; Kalk & Berendsen, 1976). The steady-state NOE for an isolated two-spin system is given by

$$\eta_{i\to j} = \sigma_{ij} T_{1j} \quad (3)$$

where T_{1j} is the selective spin–lattice relaxation time of H_j and σ_{ij} is the cross-relaxation between H_i and H_j; $\sigma_{ij} \propto r_{ij}\tau$, where r_{ij} is the interproton separation and τ is the molecular tumbling time. For strongly paramagnetic systems, the selective T_1 may be replaced by the nonselective T_1 in eq 3 (Lecomte & La Mar, 1986).

Proton NOE measurements were performed on a Nicolet NT-360 FT NMR spectrometer operating at 360 MHz in the quadrature mode using 16 384 data points collected in double precision over a 80-kHz bandwidth. The NOE experiments were performed according to the pulse sequence

$$[A(t_i\text{–}t_{on}\text{–}P\text{–Acq})_n B(t_i\text{–}t_{off}\text{–}P\text{–Acq})_n]_m$$

where A and B designate two different data files, t_i is a preparation time to allow the relaxation of the resonances (50 ms), t_{on} is the time during which the resonance is kept saturated (30 ms), and t_{off} is an equal time (30 ms) during which the decoupler is set off-resonance. P, the observe pulse, was either a 90° hard pulse (in the case of resting-state HRP) or a Redfield 2–1–4–1–2 excitation (Redfield et al., 1975) (in the case of HRP-I where the residual HOD signal is too intense because of the addition of H_2O_2). In the case of Redfield excitation, some attenuation of the transmitter power was applied to obtain a $\pi/2$ pulse at the carrier; n was set to 256, and the total number of scans in each file (nm) was (3–4) $\times 10^4$. The NOE difference spectrum was obtained by subtracting B from A. Use of the Redfield 2–1–4–1–2 pulse sequence, however, gives a narrow window of excitation, and it was not possible to excite all of the resonances evenly in the

Table I: Chemical Shifts, Assignments, and Relaxation Times for Resolved Resonances in HRP and HRP-I

peak designation	assignment	HRP[a] shift (ppm)[c]	HRP[a] T_1 (ms)[d]	HRP-I[b] shift (ppm)[c]	HRP-I[b] T_1 (ms)[e]
a	1-CH_3	67.69	7.8	51.98	9.5
b	3-CH_3	49.63	8.3	73.85	7.2
c	5-CH_3	73.73	6.9	60.46	7.5
d	8-CH_3	64.27	9.8	77.92	7.8
e	2-H_α	65.80	9.4	31.42	10.8
f	4-H_α	43.65	5.5	50.70	7.5
g	7-H_α	48.31	9.4	24.13	8.5
h	7-H'_α	31.72	6.2	15.40	
i	6-H_α	46.07	5.4	44.00	6.5
j	6-H'_α	41.58	7.4	24.70	8.5
k	His-170 H_β	38.00	2.0	21.20	2.0
l	His-170 H'_β	34.55	2.0	*f*	
s	2-$H_{\beta c}$	−5.77	8.0	−23.34	6.8
t	2-$H_{\beta t}$	*f*		−24.22	5.8
u	4-$H_{\beta c}$	*f*		−15.25	13
v	4-$H_{\beta t}$	−5.40	8.5	−12.10	14
z	Arg-38(?)	−8.35	1.0		

[a] pH 7.0, 55 °C; DSS as reference. [b] pH 7.0, 15 °C; DSS as reference. [c] Uncertainty in shift, ±0.02 ppm. [d] Uncertainty in T_1s, ±10%. [e] Uncertainty in T_1s, ±20%. [f] Not resolved from diamagnetic envelope.

spectral window (−20 to 80 ppm) needed for HRP-I. This leads to the situation that more than one experiment is necessary to obtain quantitative NOE measurements from a single peak.

There are three possible origins for nonzero intensity for peaks in an NOE difference trace, beside the one from the peak that is being on-resonance saturated (peak q): those that show an NOE to peak q, nearby resonances which are partially off-resonance saturated (indicated by the symbol ●), and peaks which are due to NOEs from the off-resonance saturated peaks (which are labeled ✦). Direct NOEs from peak q are independent of decoupler power or degree of saturation of peak q. Off-resonance saturation is approximately inversely quadratically dependent on decoupler power (Slichter, 1978), and NOEs from off-resonance saturated peaks can be easily established by saturating the peak on-resonance. Each of these controls was executed in the interpretation of each NOE difference trace. In the case of crowded spectral regions, the effects of stepping the decoupler frequency through the spectral region allowed clear differentiation between NOEs and off-resonance effects (see below).

In all of the above ^1H NMR measurements, the signal-to-noise ratio was improved by exponential apodization of the free-induction decay which introduced 50-Hz line broadening. Peak shifts were referenced to the residual water signal, which in turn was calibrated against internal 2,2-dimethyl-2-silapentane-5-sulfonate, DSS. Chemical shifts are reported in parts per million, ppm, with downfield shifts taken as positive.

Results

Spin–Lattice Relaxation. The T_1 values for HRP at 55 °C in ^2H_2O, as determined from a least-squares fit to the relaxation data from a inversion–recovery experiment, are listed in Table I. Except for the very short T_1 values for peaks l and k (~2 ms), the rest of the resolved peaks have values in the range 5.5–9.8 ms, which are comparable to the values previously reported for high-spin ferric metaquomyoglobin (Unger et al., 1985). T_1 values for the two resolved vinyl H_β peaks, s and v, were determined from the null point with the relation $T_1 = \tau_{null}/\ln 2$. The approximate T_1 of peak z is ~1 ms.

The stability of HRP-I was insufficient (half-life ~30 min) to allow determination of T_1 values by a complete inversion–recovery pulse sequence. Instead, data were collected until the peak intensities had gone through the null in each case, and the T_1 values was estimated from the relation $T_1 = \tau_{null}/\ln 2$. An insignificant amount of resting state HRP had regenerated during the time necessary to collect such data. These T_1 estimates for HRP-I at 15 °C in ^2H_2O are also listed in Table I. While the T_1 values for HRP-I therefore have larger uncertainties than for HRP, the relative T_1 values for nonequivalent HRP-I peaks should be accurately reflected in the relative values of the τ_{null} values. It is noteworthy that the T_1 values for a given functional group are very similar in resting state HRP at 55 °C and compound I at 15 °C; even the pattern of T_1 among the various substituents is maintained in the two states (see Table I).

FIGURE 1: The 360-MHz ^1H NMR spectrum of (A) 3 mM HRP in 100% ^2H_2O at 55 °C, pH 7.0. Previously assigned peaks (La Mar et al., 1980) are labeled a (1-CH_3), b (3-CH_3), c (5-CH_3), d (8-CH_3), e (2-H_α), f (4-H_α), v (4-$H_{\beta t}$), and s (2-$H_{\beta c}$). (B–G) The NOE difference spectra generated by subtracting the reference spectrum with decoupler off-resonance from a similar spectrum of the same sample in which the desired resonance was saturated for 30 ms with a 50-mW decoupler pulse. In each of the difference spectra (B–G), a downward arrow indicates the peak being saturated. Difference spectra with *y*-scale expansion are shown as inserts. (B) Saturation of peak c (5-CH_3) showing NOE to peak j. (C) Saturation of peak j showing the small reciprocal NOE to peak c and a NOE to peak i. (D) Saturate peak i; note the reciprocal NOE to peak j and a very weak NOE to peak c. (E) Saturate peak d (8-CH_3); note the NOE to peak g. (F) Irradiate peak g; note the reciprocal NOE to 8-CH_3 as well as a strong NOE to peak h. (G) Saturate peak h; note the strong (32%) reciprocal NOE to peak g and a very weak NOE to 8-CH_3. Off-resonance saturated peaks are marked (●), and NOEs from each off-resonance saturated peak is indicated by (✦).

HRP Assignments. The 360-MHz ^1H NMR spectrum of HRP in ^2H_2O is illustrated in Figure 1A, with the peaks labeled as previously assigned by selective deuteriation (La

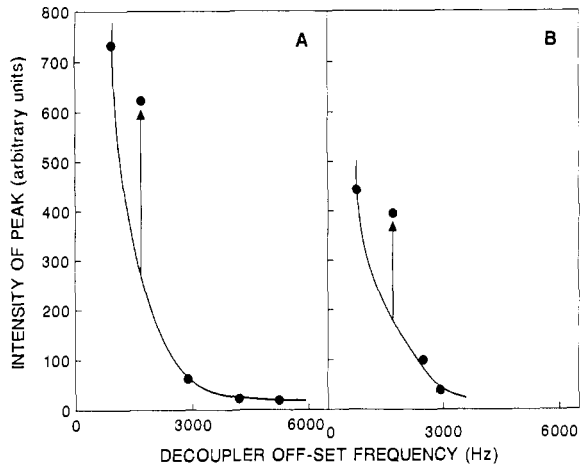

FIGURE 2: Plot of peak intensity (arbitrary units) in the NOE difference spectra versus the offset position of the decoupler radiofrequency from the peak whose intensity in the difference trace is being monitored in HRP. (A) Peak i; (B) peak j. The data points represent the intensity of the peak of interest as a function of decoupler radiofrequency offset, and the solid line shows the dependency of the intensity of the frequency offset. The data point above the smooth curve, as indicated by the vertical arrow, results when the offset frequency is set on the peak that is dipolar coupled with the peak whose intensity is being measured. Thus the enhanced intensity of the data point from the smooth curve represents the NOE to the peak of interest.

Mar et al., 1980b). The six unassigned peaks are g–l. Saturation of 5-CH_3 (c) yields a small NOE only to peak j (Figure 1B), while saturation of j (Figure 1C) gives the reciprocal small NOE (1.8%) to c, as well as a larger (~26%) NOE to peak i. Peaks marked ● are due to off-resonance saturation of peaks near the desired saturated resonance and decrease strongly in intensity when less decoupler power is used (see below). Peak i exhibits a recpirocal large (~23%) NOE to j (Figure 1D). In this trace, peaks b, g, and f are off-resonance saturated, and peaks d and h are due to NOEs from the off-resonance saturation of peak g (see Figure 1F). The unique proximity of one 6-H_α to the 5-CH_3 assigns j to one 6-H_α and i to its geminal partner.

Saturation of 8-CH_3 (d) yields a small NOE to peak g (Figure 1E), identifying g as a 7-H_α. Irradiating peak g results in a reciprocal 3% NOE to 8-CH_3 and a ~20% NOE to peak h (Figure 1F), which, when saturated in turn, yields a reciprocal large (32%) NOE to g (Figure 1G). [In trace F, peak f (4-H_α) is due to the expected NOE (Thanabal et. al., 1986) from off-resonance saturated b (3-CH_3).] This establishes that g and h arise from the 7-H_αs. The effects of saturating 1-CH_3 (a) and 3-CH_3 (b), which can be used to assign individual vinyl H_βs and determine the orientation of each vinyl, have been reported previously (Thanabal et al., 1986).

The remaining two downfield contact-shifted peaks k and l must therefore arise fom the proximal His-170 H_βs (Lauffer et al., 1983). Saturation of these peaks proved much more difficult because of their shorter T_1s, and it was not possible to observe NOEs between two such broad and closely spaced peaks. The chemical shifts and assignment of the HRP resonances, together with their T_1 values, are given in Table I.

The ability to differentiate off-resonance saturation of nearby peaks from true NOEs rests on proper controls. Off-resonance saturation is quadratic in rf decoupler power (Slichter, 1978), while NOEs are independent of such power. More directly, off-resonance effects fall off strongly with resonance position from the desired saturated peaks. Thus, a plot of peak intensity in the difference trace versus off-resonance position for 6-H_α peaks i (Figure 2A) and j (Figure 2B) reveals that their intensity due to off-resonance effects follows a smooth curve reflecting the known dependency on frequency offset, except when a peak is saturated that is dipolar coupled. The NOE is the portion above the smooth curve, as indicated by the vertical arrow.

A resolved peak which remains unassigned is peak z in Figure 1; its width and proximity to the diamagnetic envelope preclude its saturation for NOE studies. Its short T_1 (~1 ms) suggests a distance ≤4.5 Å from the iron, which, together with the upfield axial dipolar shift characteristic of high-spin ferric systems with large zero-field splitting (La Mar & Walker-Jensen, 1978), suggests one of the distal Arg-38 side-chain protons as its origin.

HRP-I Assignments. Since HRP-I was generated by the addition of H_2O_2 in H_2O, the spectrum contains a very intense residual residual H^2HO peak. In a normal ^1H NMR spectrum, the solvent line is too large to allow detection of the protein peaks, and the use of the decoupler to presaturate the water leads to artifacts in a difference spectrum that obscure useful NOEs. Thus, all HRP-I spectra had to be recorded with a Redfield (Redfield et al., 1975) pulse sequence where the solvent line is not excited.

The reference Redfield spectrum of HRP-I, optimized for the spectral window 20–80 ppm, is illustrated in Figure 3A. Heme methyl and vinyl peak assignments determined by isotope labeling (La Mar et al., 1981) are given. Deuteriation of all heme positions except the two propionate α-CH_2s has demonstrated that the only unassigned resolved contact-shifted resonances are the single proton peaks g, i, j, and k. The upfield region, which contains the assigned vinyl H_βs (La Mar et al., 1981; Thanabal et al., 1986), is not observed in this excitation window. Saturation of 5-CH_3 (c) yields a significant NOE to peak j (Figure 3B) and a much smaller one to peak i, indicating that j is the 6-H_α that is closer to 5-CH_3 and i is its geminal partner. Irradiation of i (Figure 3C) and j (Figure 3D) yield large reciprocal NOEs (22 and 28%, respectively), as well as a 3.9% NOE back to 5-CH_3. Thus, i and j originate from the 6_α-CH_2.

Saturation of 8-CH_3 (d) yields a small NOE only to peak g (Figure 3E) and identifies it as a 7-H_α. Irradiation of peak g (Figure 3F) leads to a reciprocal 2.6% NOE to 8-CH_3 but fails to yield an NOE to any other peak below 15 ppm, specifically to peak k (this is better seen in Figure 4B, see below). A weak signal is detected at 15 ppm, but the sensitivity is not satisfactory for optimal detection for this spectral window (see below). However, the absence of an NOE to peak k dictates that *k cannot arise from a heme proton.* Saturation of peak k (Figure 3G) leads only to off-resonance effects in the resolved portion of the spectrum.

The dipolar connectivity for the 7_α-CH_2 group is more clearly observed for a Redfield spectrum optimized for the spectral window 10–40 ppm (Figure 4A). Here it is observed that saturation of peak g (7-H_α) clearly leads to a large NOE to a peak at 15.4 ppm, which we designate h (Figure 4B), with the reciprocal NOE detected when h is irradiated (Figure 4C), identifying g and h as the two 7-H_αs. Saturating peak k again demonstrates the absence of NOEs to any peak outside the diamagnetic envelope. NOEs to peaks within the diamagnetic envelope cannot be detected, in part because of the nature of the Redfield pulse profile but also because of artifacts introduced by the substantial off-resonance saturation of the water signals when peaks within ~20 ppm of the solvent signal are saturated.

Discussion

Utility of NOEs. The spectra for both HRP and HRP-I clearly demonstrate that large and highly informative primary

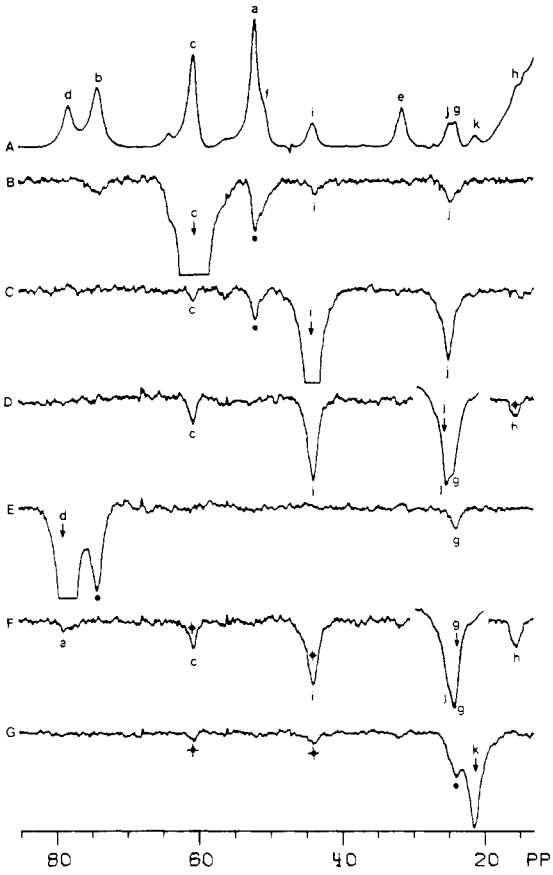

FIGURE 3: (A) The hyperfine-shifted portions of the 360-MHz ^1H spectrum of 3 mM HRP-I in 99.8% ^2H_2O at 15 °C, pH 7.0. The spectrum was collected with a Redfield 2–1–4–1–2 pulse sequence (Redfield et al., 1975) with the spectral window optimized in the region 20–80 ppm. Previously assigned peaks (La Mar et al., 1981) are labeled so that the signals from the same functional groups in HRP and HRP-I are given the same letter, i.e., a (1-CH_3), b (3-CH_3), c (5-CH_3), d (8-CH_3), e (2-H_α), and f (4-H_α). Note that the relative intensities do not correspond to the relative number of protons in some cases because of the excitation profile of the Redfield pulse train (Redfield et al., 1975) centered at 45 ppm. Thus d (8-CH_3) appears to have much less intensity than c (5-CH_3) and k less intensity than i. In an ordinary hard pulse experiment (La Mar et al., 1981), d and c, as well as i and k, have the same intensities. The NOE difference spectra (B–G) are generated as described in Figure 1. The downward arrow shows the peak being saturated; a filled circle (●) denotes off-resonance saturation, and NOEs from peaks off-resonance saturated are marked (◆). (B) Saturate peak c (5-CH_3); note the strong NOE to peak j and a weak NOE to peak i. (C) Irradiation of peak i showing a large (22%) NOE to peak j and a weak NOE to 5-CH_3. (D) Saturate peak j; note the large reciprocal NOE (28%) to peak i and also relatively strong NOE to 5-CH_3. The partial saturation of overlapping peak g results in the NOE to peak h. (E) Saturation of peak d (8-CH_3) showing NOE to peak g. (F) Saturate peak g; note the very weak NOE to 8-CH_3 and also an NOE to a peak at 15.4 ppm which is not resolved in the reference spectrum. The NOEs to peaks c and i are due to the partial saturation of the overlapping peak j (shown in the insert). (G) Saturation of peak k fails to yield any detectable NOE to the resolved signals. The weak NOEs to peaks c and i are the result of the off-resonance partial saturation of peak j.

NOEs are obtainable even in highly paramagnetic forms of HRP with very broad lines. The broad lines necessitate the use of large decoupling power which can lead to complicating off-resonance saturation. We have shown, however, that proper experimental controls clearly can differentiate between NOEs and such off-resonance effects (Figure 2). The magnitudes of the NOEs between heme methyl and neighboring protons and between the two methylene protons of each propionate are ~2–3 times larger than those previously reported

FIGURE 4: (A) Hyperfine-shifted portion of the 360-MHz ^1H NMR spectrum of 3 mM HRP-I in 99.8% ^2H_2O at 15 °C, pH 7.0. The spectrum was collected with a Redfield 2–1–4–1–2 pulse sequence with the spectral window optimized for the region 10–40 ppm. The downfield 40–80 ppm region is the second and third excitation windows of the pulse sequence, and the signals in this region have their intensity and phases according to the phase modulation of the Redfield pulse sequence (Redfield et al., 1975). Peak labeling is the same as in trace A of Figure 3. Note that peak i has opposite phase and peaks a, c, and f fall near the crossover point of the excitation windows, and hence, these resonances are not excited. (B–D) NOE difference spectra generated as described in Figure 1. The downward arrow shows the peak being saturated; a filled circle (●) denotes off-resonance effects, and (◆) signifies NOEs from off-resonance saturated peaks. (B) Saturation of peak g yielding NOEs to peaks h and d; note the NOE to peak i from the partial saturation of peak j. (C) Saturate peak h at 15.4 ppm; note the large reciprocal NOE to peak g and a weak NOE to 8-CH_3. (D) Saturation of peak k showing the absence of any NOE to the resolved signals.

(Unger et al., 1985) for the same functional groups in high-spin ferric metaquomyoglobin. This is due to the fact that the iron T_{1e} is characteristic primarily of the oxidation/spin state and independent of molecular size, while cross-relaxation, σ_{ij}, is linear in size (Noggle & Schirmer, 1971), so that eq 3 is quantitatively consistent with the larger NOEs in HRP. *Thus it can be expected that, for strongly paramagnetic proteins, NOEs should get progressively larger as the molecular size of a protein in a given iron oxidation/spin state increases.* The potential problems are lack of resolution and inability to effectively saturate peaks as they get broader.

Moreover, the observed NOE can be interpreted quantitatively. Thus for HRP, the 6_α-CH_2 NOEs, $\eta_{i\rightarrow j} \sim -0.26 = \sigma_{ij}T_{1j}$ and $\eta_{j\rightarrow i} \sim -0.23 = \sigma_{ji}T_{1i}$, are consistent with the known (Thanabal et al., 1987a) cross-relaxation rate for a methylene proton pair ($\sigma \sim -37$ Hz) and the T_1s in Table I, which predict $\eta_{i\rightarrow j} = -0.27$ and $\eta_{j\rightarrow i} = -0.20$. Similarly, the observed 7_α-CH_2 NOEs of $\eta_{g\rightarrow h} \sim -0.20$ and $\eta_{h\rightarrow g} \sim -0.32$, together with $\sigma = -37$ Hz and T_1s for peaks g and h, yield NOEs of −0.22 and −0.35, respectively. It is also noted that for HRP in neat ^2H_2O solution the different NOE spectra yield a straight base line through the diamagnetic envelope, except for the presence of selective NOEs such as to the likely propionate H_β peaks (Figure 1C,D). Thus, not surprisingly, spin diffusion to the

protein matrix (Kalk & Berendsen, 1976) is suppressed even more effectively in high-spin than low-spin ferric forms of HRP (Thanabal et al., 1987a,b, 1988).

Proximal His in HRP. The only heme resonances with line width < 1 kHz which can be expected (La Mar, 1979; Satterlee, 1986) to exhibit significant low-field hyperfine shifts (>20 ppm) in high-spin ferric hemoproteins are the heme methyls, 6- and 7-propionate H_αs, and 2- and 4-vinyl H_αs. The meso-Hs are much broader so as to be undetectable and resonate upfield of the diamagnetic envelope, as revealed by ^2H NMR of appropriately labeled hemin (G. N. La Mar, V. Thanabal, R. D. Johnson, and K. M. Smith, unpublished results). The four propionate H_βs resonate in the diamagnetic envelope (La Mar, 1979; La Mar et al., 1980b), and the four vinyl H_βs all resonate upfield of 0 ppm (Thanabal et al., 1987a). The present demonstration that peaks k and l cannot arise from the hemin dictates that they must arise from the proximal His-170 β-CH_2, inasmuch as the low-field hyperfine shifts are necessarily contact in origin (La Mar, 1979) and hence must originate from functional groups on residues directly bonded to the iron. The His-170 nonlabile ring protons are expected to have line widths in excess of 1 kHz. The positions of the two signals k and l are consistent with those found in model compounds (Lauffer et al., 1983). The NOEs between k and l are too small to establish their geminal relationship (i.e., $\eta = \sigma T_1$, and $\sigma = -37$ Hz and $T_1 \sim 2$ ms yield $\eta \sim 0.06$, which is difficult to detect for two such broad and closely spaced lines). However, we have shown elsewhere using saturation transfer from HRP to HRPCN (Thanabal et al., 1987b) and NOEs solely within HRPCN that k and l are indeed geminal partners from the His-170 β-CH_2 and that the shifts in HRPCN can be used as a probe to establish that the axial histidyl imidazole is deprotonated in the cyanide-ligated protein.

Second Oxidizing Equivalent in HRP-I. The NOE connectivities for compound I *dictate that peak k at 21 ppm does not originate from the hemin*, inasmuch as all side-chain peaks are accounted for (La Mar et al., 1981; Thanabal et al., 1986). Since all other hyperfine-shifted peaks, both upfield and downfield, arise from the hemin and magnetic anisotropy on the part of the low-spin Fe(IV) must be small (La Mar et al., 1983; Balch et al., 1985), *peak k must therefore also experience primarily a contact shift and hence must arise from an amino acid side chain, most likely the axial histidine-170.* Its 400-Hz line width precludes it from originating from the ring side chain, since these protons yield line widths ~10 times those of methyls (La Mar, 1979; La Mar et al., 1980c). The similarity of the relaxation properties of peak k relative to that of heme methyls in HRP-I at 15 °C and that of the now assigned His-170 H_βs (peaks k and l) to that of heme methyls in HRP at 55 °C argue that k arises from the same functional group in HRP and HRP-I. Hence we must conclude that it originates from a His-170 β-H. Attempts to detect a geminal partner NOE to peak k in the diamagnetic envelope were unsuccessful because of the large solvent resonance (see above).

It is noteworthy that, in spite of the very different electronic structures of HRP [Fe(III), $S = {}^5/_2$] and HRP-I [Fe(IV), $S = 1$ weakly coupled to a $S = {}^1/_2$ radical], the iron electron spin relaxation times of the former at 55 °C and the latter at 15 °C must be quite similar in order to yield such similar nuclear relaxation times (see Table I). In fact, the various heme substituents exhibit T_1s which are essentially the same in HRP and HRP-I, and reflect the distance to the iron center. Thus peak k in HRP-I, assigned to the His-170 H_β, exhibits the same shortened T_1, relative to that of a heme methyl or methylene protons, as found for peaks k and l (His-170 H_βs) in HRP.

Previous ^1H NMR studies of model compounds (Chin et al., 1980a,b; Balch et al., 1985), as well as HRP-II and ferryl myoglobin (La Mar et al., 1983; Balch et al., 1985) [all possessing oxo-bound low-spin iron(IV)], have demonstrated that the iron center cannot be responsible for the substantial axial His H_β contact shift. Our conclusions, therefore, are that the *cation radical of HRP-I is not localized solely on the porphyrin but exhibits significant delocalization to the axial histidine.* That porphyrin cation radicals can extend to axial ligands has support in the literature of model compounds, where the addition of pyridine to the zinc porphyrin cation radical leads to the appearance of nitrogen hyperfine interaction from the axial base in the radical ESR spectrum (Fujita et al., 1983). However, the present NMR data provide the first evidence that the radical may be similarly delocalized in the protein environment.

The second oxidizing equivalent in C*c*P-I is known not to be associated with the heme group (Yonetani & Ray, 1965; Poulos & Kraut, 1980; Hoffman et al., 1981). The cation radical in C*c*P-I had, at various times, been considered to reside on a tryptophan (Yonetani & Ray, 1965) (Trp-51) on the distal side of the heme, and on proximal sites involving two interacting methionines (Hoffman et al., 1979) (Met-230 and -231) or a single methionine (Hoffman et al., 1981) (Met-172). The replacement of Trp-51 and Met-172 by site-directed mutagenesis (Fishel et al., 1987; Goodin et al., 1986), leaving the radical nature unaltered, together with an X-ray crystal structure of C*c*P-I (Edwards et al., 1987) has led to the current view that the second oxidizing equivalent resides on the proximal side of the heme and may involve two methionine (Met-230 and -231) close to Trp-191. It is noteworthy that this Trp-191 is parallel to, and exhibits π–π contacts with, the proximal His imidazole ring (Finzel et al., 1984). It is thus likely that reaction of C*c*P with peroxide initially also yields a porphyrin-centered cation radical as in HRP-I, which by virtue of the presently described delocalization to the proximal His moves to the more oxidizable pair of methionenes via the "conducting" Trp-191. Unfortunately, C*c*P-I has not yielded useful ^1H NMR spectra (Satterlee & Erman, 1981) which would allow an assessment of whether either the porphyrin or the axial histidine participates in any significant extent in the delocalized radical.

Heme Side-Chain Orientation. Our preliminary NOE study of HRP and HRP-I demonstrated that irradiation of the 1-CH_3 and 3-CH_3 signals can lead to the orientation of the neighboring vinyl side chains (Thanabal et al., 1986). Thus, the resting state HRP and compound I, as well as the cyanide-ligated HRP, were shown to possess vinyls which are close to coplanar with the heme, with the 2-vinyl in the trans and the 4-vinyl in the cis configuration, as shown in structure I.

The orientation of the heme propionate side chains can be determined from a combination of the NOEs to adjacent heme methyls, their relaxation properties, and the fact that the predominant methylene proton contact shift is strongly dependent on the rotational position of the side chain (La Mar, 1973; Pande et al., 1986). Such an α-methylene proton, H_i, exhibits a contact shift, $(\Delta H/H)^i_{con}$, which is given by the relation (La Mar, 1973)

$$(\Delta H/H)^i_{con} = Q \cos^2 \phi_i \qquad (4)$$

where Q is a constant that depends on the amount of spin density on the adjacent pyrrole carbon, C_π, and ϕ_i is the angle between the C_π–CH_i plane of the methylene group and the z axis of C_π (Figure 5). Thus, the ratio of contact shift for

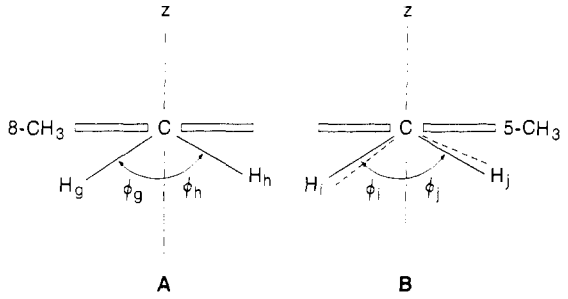

FIGURE 5: The 7-propionate (A) and 6-propionate (B) α-methylene group orientation in HRP and HRP-I as determined by the pattern of contact shifts as reflected by eq 5. The view is along the C_α–C_π axis where C_π is the appropriate pyrrole carbon for each propionate and the z axis is along the p_z axis of each of the Cp_π orbitals. The heme plane is shown as a horizontal open line. The orientation in resting state HRP is given by solid lines, and changes in orientation upon formation of compound I are indicated by broken lines. Solely the 6-propionate α-CH_2 rotates by $\sim$5° counterclockwise upon formation of HRP-I.

the two geminal methylene protons, q and r, of a propionate side chain must obey the relation

$$Z_{qr} = (\Delta H/H)_q/(\Delta H/H)_r = \cos^2 \phi_q/\cos^2 \phi_r \quad (5)$$

where, necessarily, $\phi_r = 120 - \phi_q$.

For the 7-propionate group, the contact shifts for g and h are 44.8 and 28.2 ppm, yielding $Z_{gh} = 1.6$ and $\phi_g = 56°$ and $\phi_h = 64°$, as depicted in part A of Figure 5. Upon formation of HRP-I, the 20.6 and 12.0 ppm contact shifts[2] for g and h lead to $Z = 1.6$, which dictates no change in the orientation of the 7-propionate group. For the 6-propionate group, the contact shifts for peaks i and j in HRP are 42.6 and 38.1 ppm, which gives $Z = 1.10$ and demands that $\phi_i = 59$ and $\phi_j = 61°$. Upon formation of HRP-I, the difference in contact shifts increases, and the relative magnitudes change significantly, 40.5 (i) and 21.2 (j) ppm, to yield $Z = 1.9$ so that $\phi_i = 54°$ and $\phi_j = 66°$. Thus, the 6_α-methylene group rotates counterclockwise in Figure 5B by $\sim$5° upon formation of compound I.

The NOE from the methylene proton adjacent to a methyl on a pyrrole can lead to an estimate of the mean separation. While the absolute value of the distance is not important, the relative distances between the methylene proton and the methyls support the propionate orientation determined from the contact shift pattern above. Thus, using eq 3, the −3.0% NOE from 7-H_α (g) to 8-CH_3 in HRP, together with the 8-CH_3 T_1 of $\sim$9.8 ms yields $\sigma_{ge} = -3.0$ Hz. In HRP-I, the same data yield $\sigma_{ge} = -3.3$ Hz, indicating negligible change in orientation. In the 6_α-methylene group, however, the −1.8% NOE from 6-H_α (j) to 5-CH_3 (peak c, $T_1 \sim$ 6.9 ms) yields $\sigma_{jc} = -2.6$ Hz for resting-state HRP, which in HRP-I (−3.9% NOE, $T_1 \sim$ 7.5 ms) is increased to −5.2 Hz, indicating a significant ($\sim$ 12%) decrease in the 6-H_α–5-CH_3 distance. Such a decrease in distance is consistent with the direction of the rotation determined for the ratio of contact shifts (eq 5). Thus both the change in methylene contact shift ratios and the NOEs to the adjacent methyl group argue that compound I formation for HRP is accompanied by a $\sim$5° counterclockwise rotation of the 6-propionate group, as illustrated schematically in Figure 5.

In *Cc*P both propionates point toward the protein surface, with the 6-propionate hydrogen bonded to a Lys and to several water molecules in a surface crevice (Finzel et al., 1984). Comparison of changes in propionate orientation upon formation of compound I are not readily carried out for HRP and *Cc*P, since there appears to be little structural homology in this region (Welinder, 1985). The significance of the rotation of the 6-propionate upon formation of HRP-I cannot be assessed at this time but may become apparent once an X-ray crystal structure of resting-state HRP becomes available. Since it has been shown that the cofactor, benzhydroxamic acid, makes van der Waals contact with the α-methylene protons of the 7-propionate group (Thanabal et al., 1987b), the complete absence of changes in the orientation of this side chain suggests that the substrate binding site is not significantly altered upon formation of HRP-I.

[2] A diamagnetic reference of 3.5 ppm is used for heme α-methylene groups.

ACKNOWLEDGMENTS

We are indebted to useful discussion with J. Fajer, J. T. J. Lecomte, J. D. Satterlee, and K. M. Smith.

REFERENCES

Balch, A. L., La Mar, G. N., Latos-Grazynski, L., Renner, M. W., & Thanabal, V. (1985) *J. Am. Chem. Soc. 107*, 3003–3007.

Chin, D. H., Balch, A. L., & La Mar, G. N. (1980a) *J. Am. Chem. Soc. 102*, 1446–1448.

Chin, D. H., La Mar, G. N., & Balch, A. L. (1980b) *J. Am. Chem. Soc. 102*, 4344–4350.

de Ropp, J. S., La Mar, G. N., Smith, K. M., & Langry, K. C. (1984) *J. Am. Chem. Soc. 106*, 4438–4444.

Dolphin, D., Forman, A., Borg, D. C., Fajer, J., & Felton, R. H. (1971) *Proc. Natl. Acad. Sci. U.S.A. 68*, 614–618.

Dunford, H. B. (1982) *Adv. Inorg. Biochem. 4*, 41–68.

Dunford, H. B., & Stillman, J. S. (1976) *Coord. Chem. Rev. 19*, 187–251.

Edwards, S. L., Xuong, Ng. H., Hamlin, R. C., & Kraut, J. (1987) *Biochemistry 26*, 1503–1511.

Finzel, B. C., Poulos, T. L., & Kraut, J. (1984) *J. Biol. Chem. 259*, 13027–13036.

Fishel, L. A., Villafranca, J. E., Mauro, J. M., & Kraut, J. (1987) *Biochemistry 26*, 351–360.

Freeman, R., Kempsell, S. P., & Levitt, M. H. (1976) *J. Magn. Reson. 38*, 453.

Fujita, I., Hanson, L. K., Walker, F. A., & Fajer, J. (1983) *J. Am. Chem. Soc. 105*, 3296–3300.

Goodin, D. B., Mauk, A. G., & Smith, M. (1986) *Proc. Natl. Acad. Sci. U.S.A. 83*, 1295–1299.

Hoffman, B. M., Roberts, J. E., Brown, T. G., Kang, C. H., & Margoliash, E. (1979) *Proc. Natl. Acad. Sci. U.S.A. 76*, 6132–6136.

Hoffman, B. M., Roberts, J. E., Kang, C. H., & Margoliash, E. (1981) *J. Biol. Chem. 256*, 6556–6564.

Kalk, A., & Berendsen, J. J. C. (1976) *J. Magn. Reson. 24*, 343–366.

La Mar, G. N. (1973) in *NMR of Paramagnetic Molecules* (La Mar, G. N., Horrocks, W. D., Jr., & Holm, R. H., Eds.) pp 85–126, Academic, New York.

La Mar, G. N. (1979) in *Biological Applications of Magnetic Resonance* (Shulman, R. G., Ed.) pp 305–343, Academic, New York.

La Mar, G. N., & Walker-Jensen, F. A. (1979) in *The Porphyrins* (Dolphin, D., Ed.) Vol. IV, pp 61–157, Academic, New York.

La Mar, G. N., de Ropp, J. S., Smith, K. M., & Langry, K. C. (1980a) *J. Am. Chem. Soc. 102*, 4833–4835.

La Mar, G. N., de Ropp, J. S., Smith, K. M., & Langry, K. C. (1980b) *J. Biol. Chem. 225*, 6646–6652.

La Mar, G. N., Budd, D. L., Smith, K. M., & Langry, K. C. (1980c) *J. Am. Chem. Soc. 102*, 1822–1827.

La Mar, G. N., de Ropp, J. S., Smith, K. M., & Langry, K. C. (1981) *J. Biol. Chem. 256*, 237–243.
La Mar, G. N., de Ropp, J. S., Latos-Grazynskk, L., Balch, A. L., Johnson, R. B., Smith, K. M., Parish, D. W., & Cheng, R.-J. (1983) *J. Am. Chem. Soc. 105*, 785–787.
Lauffer, R. B., Antanaitis, B. C., Aisen, P., & Que, L., Jr. (1983) *J. Biol. Chem. 258*, 14212–14218.
Lecomte, J. T. J., & La Mar, G. N. (1986) *Eur. Biophys. J. 13*, 373–381.
Morrison, M., & Schonbaum, G. R. (1976) *Annu. Rev. Biochem. 45*, 861–888.
Nicholls, P. (1962) *Biochim. Biophys. Acta 60*, 217–226.
Noggle, J. H., & Shirmer, R. E. (1971) *The Nuclear Overhauser Effect*, Academic, New York.
Pande, U., La Mar, G. N., Lecomte, J. T. J., Ascoli, F., Brunori, M., Smith, K. M., Pandey, R. K., Parish, D. W., & Thanabal, V. (1986) *Biochemistry 25*, 5638–5646.
Poulos, T. L., & Kraut, J. (1980) *J. Biol. Chem. 255*, 8199–8205.
Redfield, A. G., Kunz, S. D., & Ralph, E. E. (1975) *J. Magn. Reson. 19*, 114–117.
Sakurada, J., Takahashi, S., & Hosoya, T. (1986) *J. Biol. Chem. 261*, 9657–9662.
Satterlee, J. D. (1986) *Annu. Rep. NMR Spectrosc. 17*, 79–178.
Satterlee, J. D., & Erman, J. E. (1981) *J. Biol. Chem. 256*, 1091–1093.
Slichter, C. P. (1978) *Principles of Magnetic Resonance*, Chapter 2, Springer-Verlag, Berlin.
Thanabal, V., de Ropp, J. S., & La Mar, G. N. (1986) *J. Am. Chem. Soc. 108*, 4244–4245.
Thanabal, V., de Ropp, J. S., & La Mar, G. N. (1987a) *J. Am. Chem. Soc. 109*, 265–272.
Thanabal, V., de Ropp, J. S., & La Mar, G. N. (1987b) *J. Am. Chem. Soc. 109*, 7516–7525.
Thanabal, V., de Ropp, J. S., & La Mar, G. N. (1988) *J. Am. Chem. Soc.* (in press).
Unger, S. W., Lecomte, J. T. J., & La Mar, G. N. (1985) *J. Magn. Reson. 64*, 521–526.
Welinder, K. G. (1985) *Eur. J. Biochem. 151*, 497–504.
Yonetani, T., & Ray, G. S. (1965) *J. Biol. Chem. 240*, 4503–4508.

Two-Dimensional NMR Studies of the Porcine Muscle Adenylate Kinase†

Werner Klaus,‡ Michael Scharf, Sabine Zimmermann, and Paul Rösch*
Max-Planck-Institute for Medical Research, Department of Biophysics, Jahnstrasse 29, D-6900 Heidelberg 1, FRG
Received October 27, 1987; Revised Manuscript Received March 11, 1988

ABSTRACT: Porcine adenylate kinase was subjected to one- and two-dimensional proton NMR studies in order to identify amino acid spin systems and obtain sequence-specific resonance assignments. With a combination of results from a map of side-chain distances resulting from the refined X-ray crystallographic data and nuclear Overhauser effect spectroscopy (NOESY), assignments are suggested for all the aromatic spin systems.

Adenylate kinase (ATP:AMP phosphotransferase, AK;[1] EC 2.7.4.3) catalyzes the transfer of the terminal phosphoryl group from adenosine triphosphate to adenosine monophosphate in the presence of a divalent metal ion, physiologically Mg^{2+}, according to (Noda, 1973)

$$ATP{\cdot}Mg^{2+} + AMP \leftrightarrow ADP{\cdot}Mg^{2+} + ADP$$

The three-dimensional structure of the substrate-free porcine muscle protein (AK1) is well-known from X-ray studies (Schulz et al., 1974). The crystal structure of the yeast adenylate kinase (AK_y) loaded with the presumed bisubstrate analogue AP_5A was determined only recently (Egner et al., 1987).

Although there is plenty of evidence that the AP_5A complex of pig AK1 mimics the active structure of the enzyme, evidence for this property of the corresponding yeast or *Escherichia coli* adenylate kinase (AK_e) complex is less clear (Lienhard & Secemski, 1973; Feldhaus et al., 1975). NMR studies on the location of the nucleotide binding sites in mammalian AK1 were performed (Smith & Mildvan, 1982; Fry et al., 1985, 1987). The nucleotide sites as derived from these NMR studies are incompatible with the ones obtained from the X-ray studies of the $AK_y{\cdot}AP_5A{\cdot}Mg^{2+}$ complex crystal structure. Thus, the location of the two nucleotide binding sites is still under debate.

The NMR studies suffer from, among other things, the fact that only sequence-specific resonance assignments for the imidazole C2 proton of His^{189} and the C2 and C4 protons of the imidazole ring of His^{36} were obtained in porcine AK1 (McDonald et al., 1975; Kalbitzer et al., 1982). Several spin systems of aromatic side chains could be identified at 360 MHz (Rösch & Gross, 1985). In order to obtain more sequence-specific resonance assignments of the porcine AK1 proton NMR spectrum in the aromatic region, resolve some ambiguities in earlier work, and get spin system identifications in the aliphatic region we undertook two-dimensional NMR

† This work was supported by the Deutsche Forschungsgemeinschaft with Grants Ro617/1-1 and Ro617/1-2.
‡ Present address: Gesellschaft für biotechnologische Forschung, D-3300 Braunschweig, FRG.

[1] Abbreviations: AK, adenylate kinase (EC 2.7.4.3.); AP_5A, P^1,P^5-diadenosine pentaphosphate; COSY, correlated spectroscopy; DQF, double quantum filtered; DSS, 2,2-dimethyl-2-silapentane-5-sulfonate; NMR, nuclear magnetic resonance; NOESY, nuclear Overhauser effect spectroscopy; TOCSY, totally correlated spectroscopy; TQF, triple quantum filtered.

0006-2960/88/0427-5407$01.50/0